Precision Electroweak Physics at the Tevatron

Eric B. James
FNAL, Batavia, IL 60510, USA
on behalf of the CDF and DØ Collaborations

An overview of Tevatron electroweak measurements performed by the CDF and DØ experiments is presented. The current status and future prospects for high precision measurements of electroweak parameters and detailed studies of boson production are highlighted.

I. INTRODUCTION

The substantial samples of W and Z bosons currently being collected by the CDF and DØ experiments accommodate a wide variety of precision electroweak measurements. The two general purpose experiments observe $p\bar{p}$ collisions at a center-of-mass energy of 1.96 TeV generated by the Fermilab Tevatron Collider. In its current operating mode, the Tevatron operates as a W and Z boson factory. In a normal week of operation the Tevatron produces roughly 50,000 W boson and 5,000 Z boson events in each lepton decay channel for each experiment. Currently, each of the experiments has recorded approximately 1.5 pb^{-1} of data, which corresponds to about a quarter of the total expected Run II luminosity.

Z boson parameters have been measured to very high precision at the large electron-positron collider (LEP) at CERN and the linear collider at SLAC. For example, the Z boson mass has been measured with an accuracy of 2 parts in 10^5 [1]. However, current measurements of the W boson parameters are less precise (the present uncertainty on the W boson mass is about 4 parts in 10^4 [1]). Based on expected Run II integrated luminosities, the two Tevatron experiments will collect a sample of W bosons events on the same order as the 17 million Z boson events collected by the four LEP experiments. Using these event samples, CDF and DØ will significantly reduce the current experimental uncertainties on the electroweak parameters associated with the W boson.

In addition, the large W and Z boson samples allow for precision tests of the QCD production mechanisms for bosons. In particular, the cross section for boson production depends on both the calculable hard scattering parton cross sections and the Parton Distribution Functions (PDFs), which describe the momentum fractions carried by the quarks and gluons within the proton. The PDFs are determined experimentally, and studies of boson production at the Tevatron can be used to place constraints on these distributions. These constraints are important because PDF uncertainties significantly impact the level of precision of Tevatron measurements of electroweak parameters.

II. DETECTORS

The CDF and DØ detectors are designed to trigger on and accurately reconstruct charged particles, electrons, photons, muons, hadronic jets, and the transverse energy imbalance associated with neutrinos. The z-axes of the CDF and DØ coordinate systems are defined to be along the direction of the incoming protons. Particle trajectories are described by θ, the polar angle relative to the incoming proton beam, and ϕ, the azimuthal angle about the beam axis. Pseudorapidity, $\eta = -\ln(\tan(\theta/2))$, is also used to describe locations within the detectors.

One particular strength of the CDF detector is its beam-constrained central tracking resolution,

$$\delta(p_T)/p_T \sim 0.0005 \times p_T \text{ (GeV/}c\text{)} \; [|\eta| < 1], \qquad (1)$$

based on hit information from the outer open-cell drift chamber. The calorimeters of both detectors allow for high-resolution reconstruction of the energies of electrons, photons, and jets. For example, the energy resolution for clusters in the CDF central electromagnetic calorimeter is

$$\delta(E_T)/E_T \sim 13.5\% \oplus 1.5\% \text{ (GeV)} \; [|\eta| < 1.1], \qquad (2)$$

which allows for high precision electron energy measurements. A main strength of the DØ detector is the forward coverage provided by its calorimeters and muon detector systems. The DØ calorimeter provides hermetic coverage up to $|\eta| < 4.2$ (compared to $|\eta| < 3.6$ for CDF) and muon coverage up to $|\eta| < 2.0$ (compared to $|\eta| < 1.5$ for CDF). This additional forward coverage results in a significantly better acceptance for leptons from boson decays, particularly for muons.

III. MEASUREMENTS OF ELECTROWEAK PARAMETERS

A. W Boson Mass Measurement

A precision measurement of the W boson mass is among the highest priorities for the Tevatron experiments. Self-energy corrections to the W boson depend on the masses of the top quark ($\propto M_{top}^2$) and the Higgs

TABLE I: Preliminary uncertainty estimates for CDF W boson mass measurement using 200 pb^{-1} of data.

Uncertainty [MeV]	**Electrons**	**Muons**	**Common**
Lepton Energy Scale and Resolution	27	17	17
Recoil Scale and Resolution	14	12	12
Backgrounds	7	9	-
Production and Decay Model	16	17	16
Statistics	48	53	-
Total	60	60	26

boson ($\propto \ln M_H$), as well as potential contributions from non-Standard Model (SM) physics. Because of these dependencies, the W boson mass is a critical input to SM fits that constrain the mass of an unobserved Higgs boson or, subsequent to a potential Higgs discovery, test the consistency of the SM.

The current level of uncertainty on top quark mass measurements from the Tevatron experiments [2] is at the level of 2.1 GeV/c^2 which corresponds to roughly a 1.2 % measurement of M_{top}. To obtain equivalent constraining power on M_H, the W boson mass would need to be measured to about 0.015 % corresponding to a total uncertainty of about 12 MeV/c^2. Due to the needed level of precision, the W boson mass measurement is extremely challenging.

In order to make a measurement substantially better than 0.1 %, all aspects of W boson production and detection need to be understood at the 10 MeV level. In particular, this precision must be achieved for W boson production and decay, lepton momentum/energy scales and resolutions, and additional energies within the event associated with hadronic recoil against the boson p_T and underlying interactions of the remnant quarks and gluons. Once this detailed event model has been constructed, the W boson mass can be determined by generating events for many different mass values and picking the set that provides the best match with data, in particular by fitting to the transverse mass, $M_T = E_T^\ell E_T^\nu - (E_x^\ell E_x^\nu + E_y^\ell E_y^\nu)$, distribution for the $W \to \ell\nu$ candidate events in data.

The CDF experiment is close to completing a W mass measurement using 200 pb^{-1} of data collected at the beginning of Run II. The expected uncertainties associated with this measurement are shown in Table I. The total uncertainty for the combined measurement based on events collected in both the electron and muon channels is expected to be 48 MeV/c^2 which would make this measurement the single most precise to date. More importantly, the largest component of the total uncertainty is statistical, indicating that the result will be further improved simply by incorporating more data. In fact, with the exception of the uncertainty associated with the production and decay model, each of the uncertainty categories improves with additional statistics. Larger samples of J/Ψ, Υ, and Z boson events, for example, further improve the measurement of the track momentum and calorimeter energy scales for leptons.

Figure 1 shows a projection for the expected precision of the W boson mass measurement as a function of integrated luminosity for a single experiment based on Tevatron Run I measurements. The combined preliminary uncertainty for the 200 pb^{-1} CDF Run II analysis lies significantly below the expectation based on the Run I results, indicating improved understanding of the W boson event characteristics. With enough additional luminosity, the precision of the measurement will become limited by the uncertainties associated with the boson production and decay model (currently on the order of 20 MeV) which do not scale with statistics. Reducing these uncertainties requires additional measurements that can constrain components of the production model, such as PDFs and the boson p_T spectrum.

A projection for the potential Tevatron constraints on the Higgs boson mass based on 8 fb^{-1} of data delivered to each experiment is shown in Figure 2. At the expected level of precision, significant constraints will be placed on non-SM particles such as those predicted by supersymmetry (SUSY).

B. W Boson Width Measurements

The width of the W boson is a less constraining observable in global electroweak fits than the mass, but measuring its value confirms a basic prediction of the SM and could provide indications of new physics beyond the SM. The Tevatron experiments make both direct and indirect W boson width measurements. The direct measurements have no built-in SM assumptions and are therefore sensitive to potential contributions from new physics such as a heavy W'. Indirect measurements are based on SM assumptions and provide high precision results that can also be used to place constraints on other SM parameters such as CKM matrix elements.

Tevatron direct measurements of the W boson width are extracted from the shape of the high M_T region in $W \to \ell\nu$ events. The procedure is similar to that used for measuring the W mass. The W boson production and detector resolution effects that distort the observed lineshape must be carefully modeled within a fast event simulation. Using the tuned simulation, event samples are generated based on a range of input values for the W boson width. The change in the shape of the high M_T tail as a function of the W width is illustrated in Figure 3. DØ has made a preliminary direct measurement of the W width based

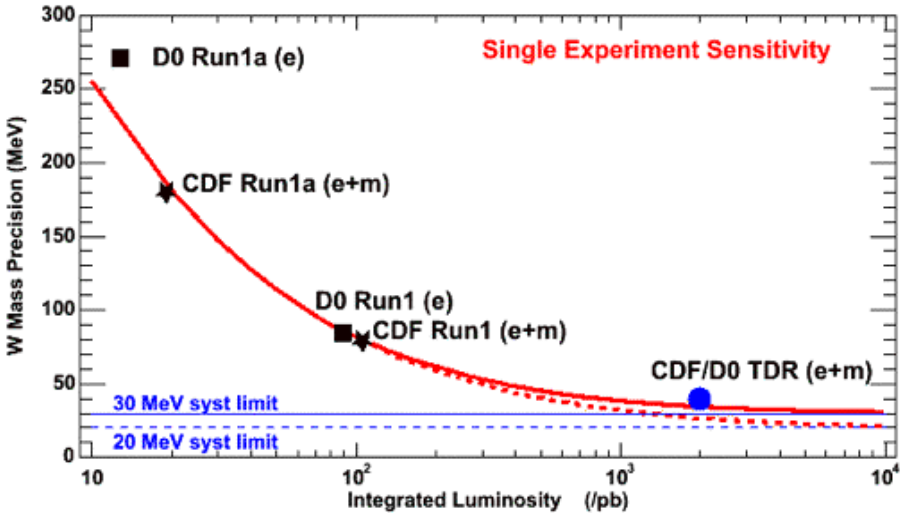

FIG. 1: Projection for the expected precision of a single experiment W mass measurement as a function of integrated luminosity based on Run I Tevatron measurements.

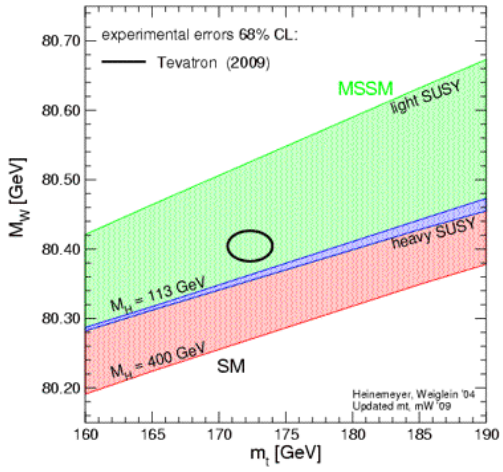

FIG. 2: Projection for Tevatron constraints on M_H based on the expected precision of combined top quark and W boson mass measurements assuming 8 fb^{-1} of data collected by each experiment.

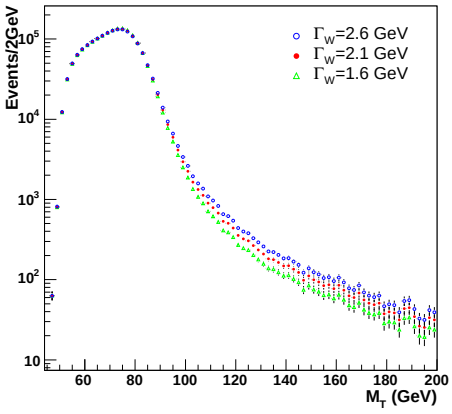

FIG. 3: DØ simulation of the M_T distribution for $W \to e\nu$ events as a function of W boson width.

on 177 pb^{-1} of Run II data. The measurement uses the peak region in the M_T distribution for $W \to e\nu$ candidate events to normalize signal and background contributions to the sample, and then fits the shape in the tail region to determine the most likely value for the W width. The final result for the W width obtained from the fit shown in Figure 4 is

$$\Gamma_W = 2.011 \pm 0.093(\text{stat}) \pm 0.107(\text{syst}) \text{ GeV}. \quad (3)$$

Indirect determinations of the W boson width are obtained from a measured ratio of production cross sections times branching fractions,

$$R = \frac{\sigma \times \text{Br}(W \to \ell\nu)}{\sigma \times \text{Br}(Z \to \ell\ell)}. \quad (4)$$

The value of R can be measured very precisely since many of the uncertainties associated with the individual cross section measurements, in particular the significant uncertainty on the measured luminosity, cancel in the ratio. Within the context of the SM, this ratio can also be expressed as

$$R = \frac{\sigma(W)}{\sigma(Z)} \times \frac{\Gamma(W \to \ell\nu)}{\Gamma(W)} \times \frac{\Gamma(Z)}{\Gamma(Z \to \ell\ell)}. \quad (5)$$

Using this equation, a precise value for $\Gamma(W)$ can be extracted from R using a next-to-next-to-leading

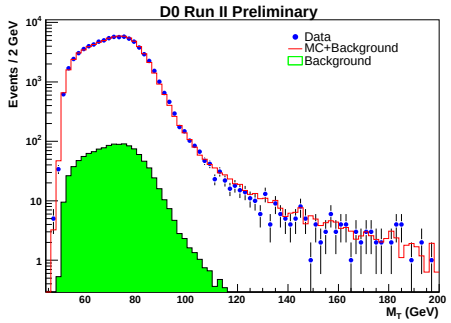

FIG. 4: DØ fit to the M_T distribution of $W \to e\nu$ events used to measure the W width.

order (NNLO) theoretical prediction for $\sigma(W)/\sigma(Z)$, precision LEP measurements of $\Gamma(Z \to \ell\ell)$ and $\Gamma(Z)$, and a SM calculation for $\Gamma(W \to \ell\nu)$.

CDF has made an indirect measurement of the W boson width based on the first 72 pb^{-1} of data collected in Run II. The ratio R was measured independently in the electron and muon channels, resulting in a combined value of

$$R = 10.84 \pm 0.15(\text{stat}) \pm 0.14(\text{syst}), \qquad (6)$$

which has an overall relative precision of 1.9 %. Since the most significant contribution to the systematic uncertainty on this measurement originates from the lepton selection efficiency measurement made from the $Z \to \ell\ell$ data samples, it is expected that a measurement with a precision of better than 1 % will be possible using additional data statistics.

The indirect value for the W boson width extracted from the measured value of R is

$$\Gamma(W) = 2092 \pm 42 \text{ MeV}, \qquad (7)$$

which is in good agreement with the SM prediction and the previously described direct measurement of the W boson width. A comparison of the measured indirect width with previous results and the SM expectation is shown in Figure 5. Since in the SM the total W boson width is a sum over partial widths for leptons and quarks, which in the case of the quarks depend on certain CKM matrix elements, the measured value of $\Gamma(W)$ can also be used to indirectly measure the value of the least constrained element, V_{cs}. Based on world-averaged measurements of the other CKM matrix elements that contribute to the partial widths, CDF obtains a value of

$$|V_{cs}| = 0.976 \pm 0.030. \qquad (8)$$

C. Quark Couplings

The Tevatron experiments can extract the axial and vector neutral current light quark couplings from measurements of the Drell-Yan forward-backward asymmetry. This asymmetry is defined as

$$A_{FB} = \frac{\sigma_F - \sigma_B}{\sigma_F + \sigma_B} \qquad (9)$$

where $\sigma_{F(B)}$ is defined as the cross section for Drell-Yan events in which the positively charged lepton is produced along (opposite) the proton's direction of motion in the parton-parton center of mass frame. The decay of the γ^*/Z in this frame is illustrated in Figure 6. The sign of $\cos(\theta^*)$ determines whether a given event is forward or backward (forward if $\cos(\theta^*) > 0$).

CDF and DØ have both made preliminary measurements of the forward-backward asymmetry for $\gamma^*/Z \to ee$ events as a function of dielectron invariant mass. The CDF result based on a 364 pb^{-1} data sample is shown in Figure 7 and the DØ result based on a 177 pb^{-1} data sample is shown in Figure 8. As illustrated in Figure 9, the quark couplings to the Z boson can be extracted from these measurements. Although

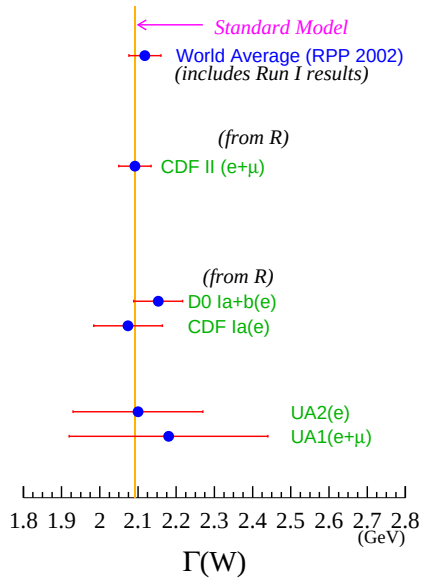

FIG. 5: Comparison of the CDF indirect width measurement with previous results and the SM prediction.

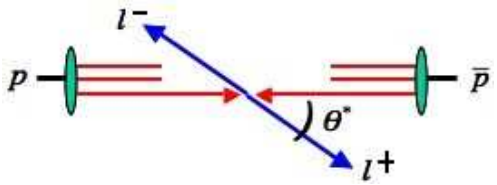

FIG. 6: Illustration of γ^*/Z decay in the parton-parton center of mass frame. Forward (backward) events are defined as those with positive (negative) $cos(\theta^*)$.

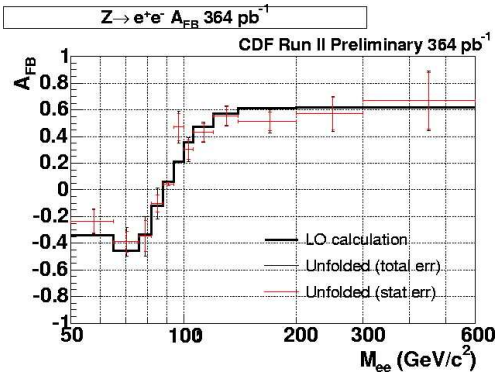

FIG. 7: CDF Measurement of the forward-backward asymmetry in $\gamma^*/Z \to ee$ events as a function of the di-electron invariant mass.

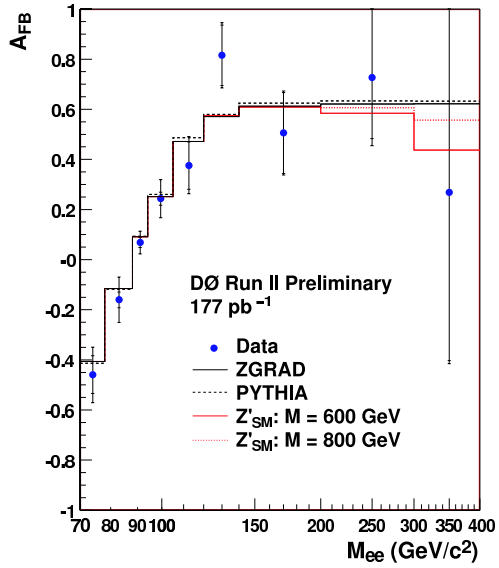

FIG. 8: DØ Measurement of the forward-backward asymmetry in $\gamma^*/Z \to ee$ events as a function of the di-electron invariant mass.

the coupling measurement is less precise than that of the LEP experiments, it breaks a two-fold degeneracy in the LEP results, providing an important confirmation of the SM. The coupling values have also been determined from analysis of deep inelastic scattering data at HERA [3].

More importantly, the Tevatron experiments measure A_{FB} over a wide range of invariant masses (both below and above the Z-pole). The high mass region is of particular interest since the effects of new bosons interfering with the SM bosons could result in measured values of A_{FB} inconsistent with SM expectations. The potential effect of a Z' on the predicted A_{FB} in the high mass region is shown in Figure 8, along with the measured DØ values. With additional data it should be possible to distinguish between the new physics and SM scenarios.

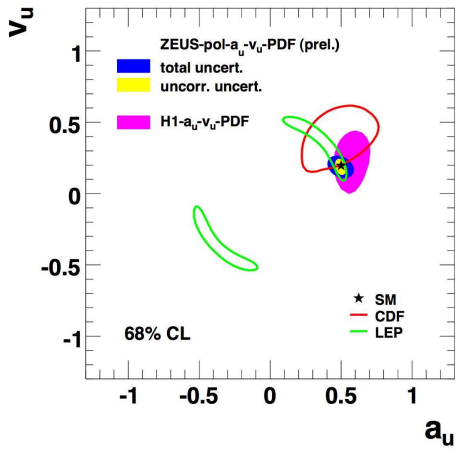

FIG. 9: Comparison of the limits on the allowed range of values for the up quark axial and vector neutral current couplings obtained from Tevatron (72 pb^{-1}), HERA, and LEP measurements.

TABLE II: Diboson final states available at the Tevatron and the trilinear couplings involved in their production. The couplings shown in parentheses are absent in the SM.

Diboson Final State	Trilinear Couplings
$q\bar{q}' \to W \to W\gamma$	$WW\gamma$ only
$q\bar{q}' \to W \to WZ$	WWZ only
$q\bar{q} \to \gamma^*/Z \to WW$	$WW\gamma$, WWZ
$q\bar{q} \to \gamma^*/Z \to Z\gamma$	$(ZZ\gamma)$, $(Z\gamma\gamma)$
$q\bar{q} \to \gamma^*/Z \to ZZ$	$(ZZ\gamma)$, (ZZZ)

D. Trilinear Gauge Couplings

The analysis of diboson final states at the Tevatron provides an opportunity for studying self-interactions of the gauge bosons. These interactions are a direct result of the electroweak SU(2) structure, and the SM makes specific predictions on the expected production cross sections for each diboson final state. Non-SM particles that couple to the electroweak bosons can modify the expected cross sections, particularly at high E_T, and looking for potential indications of these anomalous couplings provides a route to uncovering new physics.

Table II gives a summary of the diboson final states available at the Tevatron and the trilinear gauge couplings that contribute to the production of each state. The Tevatron experiments are sensitive to different combinations of couplings than LEP and explore a higher $\sqrt{s}$. The couplings in the table that are enclosed within parentheses are absent in the SM. Due to the absence of these couplings, the associated final states are ideal channels for observing effects from

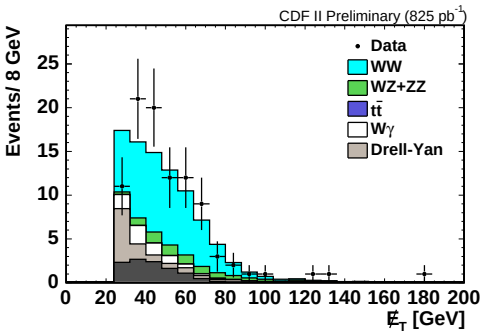

FIG. 10: Comparison of missing E_T distribution for observed data events to the combined expectation from signal and background in the CDF WW analysis.

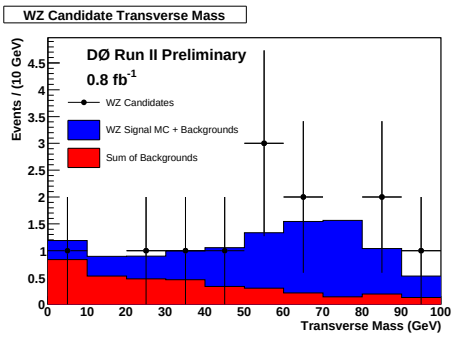

FIG. 11: Comparison of M_T distribution determined from the W boson decay products for observed data events with the combined expectation from signal and background in the DØ WZ analysis.

new physics.

The CDF and DØ experiments have produced a wide variety of new Run II results based on the study of diboson final states [4] [5]. A few of these are highlighted in detail here. The cross section for WW production, which involves both the $WW\gamma$ and WWZ trilinear gauge couplings, has recently been measured by CDF using a 825 pb^{-1} data sample. The analysis focuses on the dilepton final state produced when both W bosons decay into a lepton and neutrino. Events are selected with two opposite-sign leptons (electrons or muons) that satisfy the standard CDF selection criteria. The missing E_T in the event, expected from the two neutrinos, is required to be above 25 GeV, greatly reducing the main expected background contributions from Drell-Yan, $W\gamma$, and W plus jet production. Before looking at the signal region, events in the low missing E_T region are utilized to cross-check the background estimation. In the signal region, the final background estimate is 38 ± 5 events on top of an expected WW signal contribution of 52 ± 4 events. Based on 95 observed events, CDF measures a cross section of

$$\sigma(p\bar{p} \to WW) = 13.6 \pm 3.0(\text{stat} + \text{syst} + \text{lum}), \quad (10)$$

consistent with the next-to-leading order (NLO) calculation [6] of 12.4 ± 0.8 pb. The final candidate events plotted as a function of event missing E_T, along with the expected signal and background contributions, are shown in Figure 10.

Both CDF and DØ have also recently completed measurements of WZ production. Production of this final state is of particular interest because the WWZ coupling can be studied independent of the $WW\gamma$ coupling, which also contributes to WW production. DØ has performed a search based on a data sample corresponding to roughly 800 pb^{-1} of integrated luminosity. This analysis uses the trilepton final state in which both bosons decay leptonically. A total of three leptons (electrons or muons) passing the standard DØ selection criteria are required. Of the three leptons, two are required to be of the same flavor and form an opposite-sign pair with an invariant mass consistent with the Z boson mass. The event missing E_T is also required to be greater than 20 GeV, consistent with that from the neutrino produced in the decay of the W boson. Taking advantage of its wider acceptance for leptons, DØ expects to see 7.5 ± 1.2 signal events on top of a background of 3.6 ± 0.2 events, and observes 12 events in the data. Based on the calculated probability for the background to fluctuate into the observed number of events, DØ obtains 3.3 σ evidence for WZ production and measures

$$\sigma(p\bar{p} \to WZ) = 4.0^{+1.9}_{-1.5}(\text{stat} + \text{syst} + \text{lum}), \quad (11)$$

consistent with the NLO calculation [6] of 3.68 ± 0.25 pb. Figure 11 shows the transverse mass distribution for the neutrino (missing E_T) and lepton coming from the W boson decay for the DØ candidate events compared to the combined expectation from signal and background.

CDF completed a similar search using roughly the same amount of data and observed only 2 events compared to an expectation of 3.7 ± 0.3 signal and 0.9 ± 0.3 background events. The observation of two events was found to be consistent with both the background-only and background plus signal hypotheses. The smaller number of expected events as compared with the DØ analysis is directly related to the reduced acceptance for leptons in the CDF detector. In order to improve the CDF analysis, new lepton categories were created to take advantage of additional tracking and calorimeter cluster information in the events to increase lepton acceptance. In order to increase electron coverage out to $|\eta| < 2.8$, a category for forward electron candidates in the calorimeter with no track match was added. Similarly, an increase in muon coverage out to $|\eta| < 1.6$ was obtained using forward track candidates fiducial to the calorimeter with energy deposits consistent with the expectation from a minimum-ionizing particle. In addition, the tracks pointing at calorime-

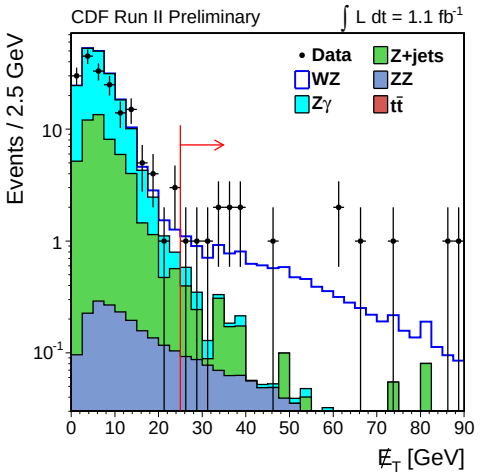

FIG. 12: Comparison of missing E_T distribution for observed data events with the combined expectation from signal and background in the CDF WZ analysis. The arrow on the figure indicates the signal region for this search (missing $E_T > 25$ GeV).

ter cracks were placed into a flavor-neutral category of leptons which could be assigned as either electrons or muons. With the additional lepton categories in place, CDF performed a new search for WZ production using 1.1 fb^{-1} of data. Including the improved lepton acceptance, CDF observes 16 events with signal and background expectations of 12.5 ± 0.9 events and 2.7 ± 0.4 events, respectively. Based on the probability of the background fluctuating into the observed signal, CDF obtains a 5.9 σ observation of WZ production and measures

$$\sigma(p\bar{p} \to WZ) = 5.0^{+1.8}_{-1.6}(\text{stat} + \text{syst} + \text{lum}), \qquad (12)$$

which is also consistent with the NLO calculation. The final candidate events plotted as a function of event missing E_T, along with the expected signal and background contributions, are shown in Figure 12.

As mentioned previously, diboson production is sensitive to new physics appearing in the trilinear gauge couplings. Potential new physics contributions can be incorporated in the Lagrangian using a standard methodology that introduces two parameters, λ and $\Delta\kappa$, which are zero in the SM and non-zero in the case of additional new physics contributions. Generally, the effect of anomalous couplings on diboson production is a net increase in the cross section at high E_T. Figure 13 illustrates how the shape of the diboson cross section as a function of E_T varies for different values of λ and $\Delta\kappa$. The added terms in the Lagrangian violate unitarity unless an upper limit (Λ) on the scale for the new physics is imposed. A common approach is to use the parameterization $\alpha(s) = \alpha_0/(1 + s/\Lambda^2)^2$ which causes the effect of the anomalous couplings to "turn-off" as the upper limit on the energy scale is approached.

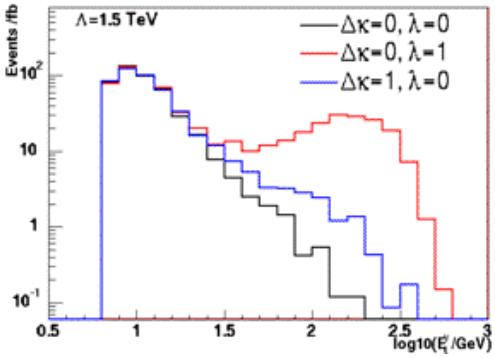

FIG. 13: The predicted shape of a generic diboson cross section as a function of E_T for different values of λ and $\Delta\kappa$.

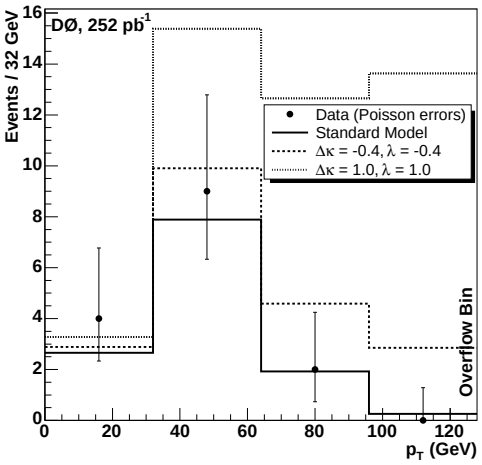

FIG. 14: Comparison of leading lepton p_T distribution for DØ WW candidate events observed in the dilepton final state with SM and non-SM expectations.

DØ has performed a preliminary analysis to set anomalous couplings limits based on a measurement of the WW cross section using dilepton final states. The analysis sets limits on anomalous $WW\gamma$ and WWZ trilinear gauge couplings under the assumption that the two couplings are equal and $\Lambda = 2$ TeV. Figure 14 shows the DØ data and both SM and non-SM expectations plotted as a function of the p_T of the highest p_T lepton. Based on the observed agreement between data and the SM prediction, DØ obtains the following limits:

$$-0.32 < \Delta\kappa < 0.45, -0.29 < \lambda < 0.45. \qquad (13)$$

These preliminary limits can be improved significantly with larger data samples and incorporating information from other final states.

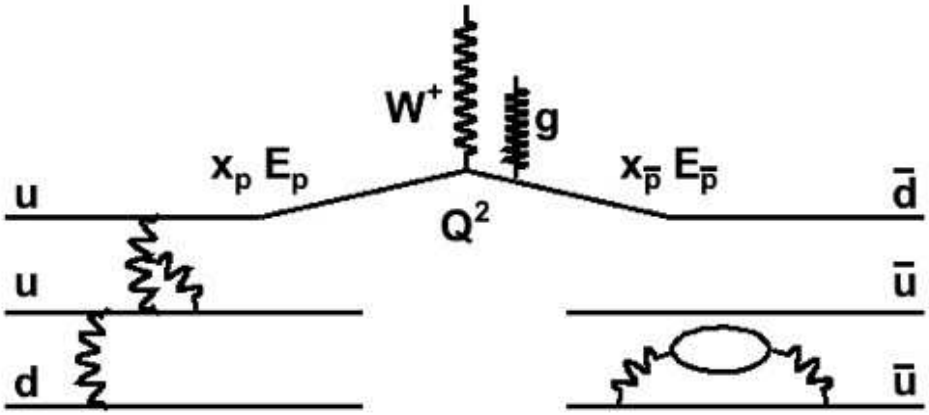

FIG. 15: Illustration of W boson production at the Tevatron. A u quark in the proton annihilates with a $\bar{d}$ quark in the anti-proton at a squared center of mass $s = Q^2$ to produce a W^+. The energies of the u and $\bar{d}$ are $x_p E_p$ and $x_{\bar{p}} E_{\bar{p}}$, respectively.

IV. STUDIES OF BOSON PRODUCTION

A. Boson Production at the Tevatron

A typical example of boson production at the Tevatron is shown in Figure 15. At leading order (LO), a quark and anti-quark pair annihilate to create a W or Z boson, which subsequently decays into a quark or lepton pair. The production cross section is calculated as a sum of partial cross sections ($d\sigma_{q\bar{q}}$), convoluted with the PDFs that describe the distributions of the proton momentum fraction (x_p) carried by each of the constituent quarks and gluons. The cross section can be written as

$$\sigma = \int \sum_{i,j} [f_i^q(x_p) f_j^{\bar{q}}(x_{\bar{p}}) + f_i^{\bar{q}}(x_p) f_j^q(x_{\bar{p}})] \times d\sigma_{q\bar{q}} dx_p dx_{\bar{p}} \quad (14)$$

where i and j denote the different possible quark flavor combinations. The longitudinal momentum of the produced boson is directly related to the PDFs. In particular, if one of the two annihilating quarks carries a significantly larger fraction of proton momentum, the boson will be produced with momentum in the same direction as the incident proton.

The effects of QCD and QED NLO corrections are also important. QCD corrections give rise to final states that contain multiple partons, sometimes with high p_T, and modify the overall boson production kinematics, including the boson p_T spectrum. The most important effect originating from NLO QED corrections is photon radiation from final state charged leptons, which have a significant effect on lepton identification and kinematics. QED radiation from the initial state quarks and from the boson itself (in the case of W bosons) also contributes to the overall event kinematics.

B. Parton Distribution Functions

The functional forms of the PDFs originate from non-perturbative QCD interactions and are therefore incalculable. Instead, they are parameterized using data from deep inelastic scattering, fixed target, and hadron collider experiments. Two standard parameterizations come from the CTEQ [7] and MRST [8] groups. In the case of the CTEQ group, the parton momentum fraction distributions are parameterized as

$$x f_a(x, Q_0) = A_0 x^{A_1} (1-x)^{A_2} e^{A_3 x} (1 + A_4 x)^{A_5} \quad (15)$$

for five categories of quark/gluon proton constituents (valence u and d quarks, sea $\bar{u}$ and $\bar{d}$ quark combinations, and gluons). This configuration gives a total of thirty free parameters in the fit to the experimental data, although the CTEQ group chooses to leave ten of these at fixed values. The remaining free parameters are determined for a low energy scale, $Q_0 = 1.3$ GeV, and the Q^2 dependence is obtained from QCD evolution equations.

A recent development is that each group also provides a set of "error" PDFs that are intended to map out the allowable parameter space for the PDFs within the experimental data uncertainties. The twenty free parameters used in the fit are found to be correlated with one another. To facilitate uncertainty calculations, these correlations are removed by forming eigenvectors within the A_i-space. For each of the twenty eigenvectors, two complete PDF sets are generated corresponding to a given increase in χ^2 of the overall fit ($\Delta\chi^2 = 100$ for the CTEQ group). The MRST group follows a similar procedure using a slightly different parameterization that results in only fifteen free parameters for their fit. The MRST group also uses a

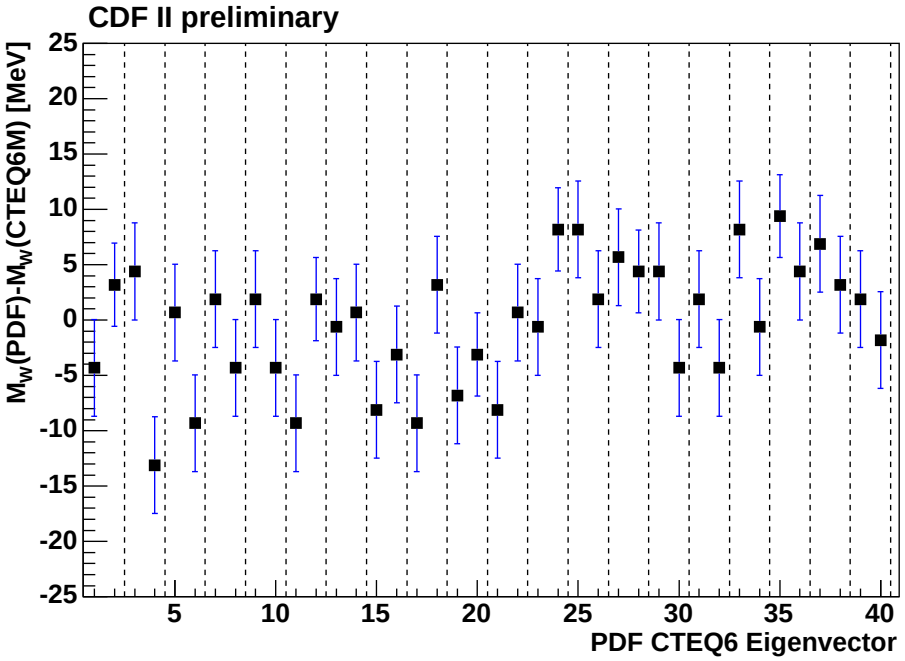

FIG. 16: An example of how CTEQ "error" PDF sets are used to determine an overall PDF uncertainty. The shift in the measured W boson mass from its central value is obtained for Monte Carlo templates generated with each of the 40 error PDF sets. The observed shifts associated with each of the twenty orthogonal eigenvectors are added in quadrature to determine the total uncertainty.

smaller $\Delta\chi^2 = 50$ to construct its version of the error PDFs.

An example of how error PDFs are used to determine an overall PDF uncertainty for a specific analysis is shown in Figure 16 for the case of the W boson mass measurement. The shift in the measured mass from its central value is obtained using Monte Carlo templates generated with each of the forty error PDF sets. Since the twenty eigenvectors are orthogonal to each other by design, the observed shifts associated with each can be added in quadrature to determine a total PDF model uncertainty. Although each eigenvector typically contains information about multiple fit parameters, there is a strong correlation in some cases between a given fit parameter and an eigenfunction. For example, the eigenvector corresponding to error PDFs 1 and 2 in Figure 16 has a significant correlation with the A_1 (low-x_p) parameter associated with valence u quarks. These correlations give an indication of the experimental inputs to the fits which need to be improved to reduce the overall PDF uncertainty for a specific analysis.

C. Inclusive Production Cross Sections

Because many electroweak measurements at the Tevatron are sensitive to uncertainties in the PDF model, both CDF and DØ perform studies of boson production to constrain the PDF model. The simplest of these studies are measurements of the inclusive boson production cross sections. The Tevatron experiments measure inclusive W and Z cross sections using each of the lepton (e, μ, and τ) decay channels. The dominant uncertainty in these results is associated with the integrated luminosity measurements made by each experiment ($\sim 6\%$). Within this uncertainty, the measured cross sections are found to be in good agreement with the NNLO theoretical calculations [9]. The agreement between CDF and DØ measured values and theoretical predications are shown in Figures 17 and 18. Since the theoretical uncertainties are significantly smaller than the measurement uncertainties, no additional constraints on the boson production model can be obtained from these measurements.

D. Forward W Boson Cross Section

Differential cross section measurements contain additional information that can be used to constrain PDFs. CDF performs a simple differential measurement by independently evaluating the W boson cross section using $W \to e\nu$ events with electrons observed in the central and forward regions of the detector. Figure 19 shows the W boson acceptance as a function

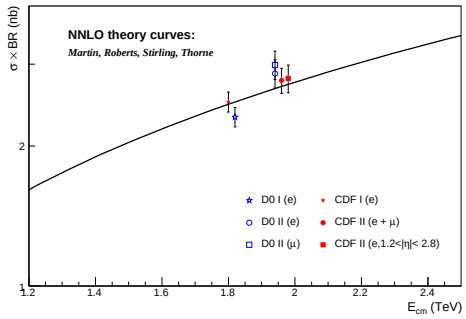

FIG. 17: Summary of Tevatron inclusive W boson cross section measurements as a function of E_{CM} compared to a NNLO theoretical calculation (solid black line).

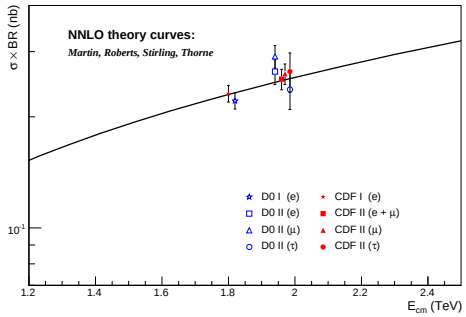

FIG. 18: Summary of Tevatron inclusive Z boson cross section measurements as a function of E_{CM} compared to a NNLO theoretical calculation (solid black line).

of the boson rapidity, defined as

$$y_W = \frac{1}{2}\log\frac{E+p_z}{E-p_z}, \qquad (16)$$

for the CDF $W \to e\nu$ cross section measurements using events with electrons reconstructed in the central and forward calorimeter modules. Since W bosons produced at different rapidities probe different regions of x_p, the ratio of central to forward cross sections measurements can be a useful tool for placing constraints on PDFs.

The selection of forward electron candidates is based on electromagnetic clusters in the calorimeter matched with tracks reconstructed primarily from silicon detector hits [10]. Given the selection criteria, CDF observes 48,165 candidate events in a 223 pb^{-1} data sample. The M_T spectrum of the candidate events is shown in Figure 20, along with the combined expectation for signal and background. The observed agreement indicates a good understanding of the forward detector systems.

The measured forward ($1.2 < |\eta_e^{det}| < 2.8$) cross section is

$$\sigma^{for} = 2796 \pm 13(\text{stat})^{+95}_{-90}(\text{syst}) \text{ pb}, \qquad (17)$$

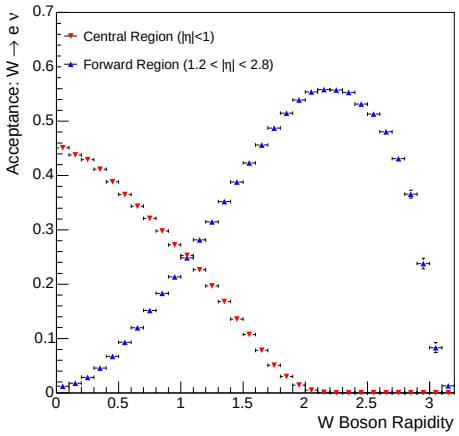

FIG. 19: W boson acceptance as a function of rapidity for the CDF $W \to e\nu$ cross section measurements using events with reconstructed electrons in the central and forward parts of the detector.

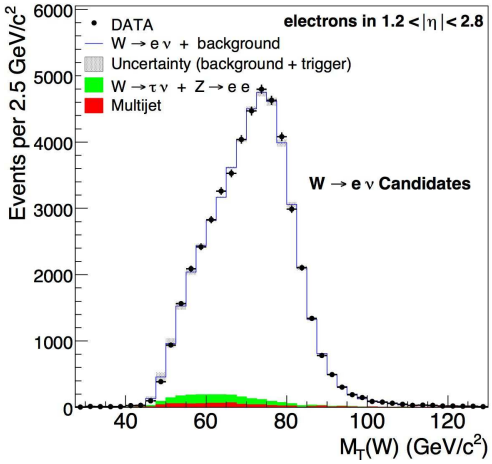

FIG. 20: M_T distribution for candidate events in the CDF cross section measurement based on $W \to e\nu$ events with electrons in the forward detector region.

neglecting the luminosity uncertainty which will cancel in the cross section ratio. The previously measured central ($|\eta_e^{det}| < 0.9$) cross section [11] has a value of

$$\sigma^{cen} = 2771 \pm 14(\text{stat})^{+62}_{-56}(\text{syst}) \text{ pb}, \qquad (18)$$

also neglecting the luminosity uncertainty. The remaining systematic uncertainties on the measurements are dominated by those associated with electron identification and the PDF model. In order to separate these, CDF uses visible cross sections, defined as

$$\sigma_{vis} = \sigma_{tot} \times A, \qquad (19)$$

where A^{cen} is for example the kinematic and geometric acceptance for $W \to e\nu$ events in the central cross

section measurement. Using this definition the PDF model uncertainties are removed from the measured ratio of cross sections,

$$R_{exp} = \sigma_{vis}^{cen}/\sigma_{vis}^{for} = 0.925 \pm 0.033. \quad (20)$$

CDF then compares the measured ratio with the equivalent theoretical ratio of acceptances

$$R_{th} = A^{cen}/A^{for} \quad (21)$$

determined from simulated event samples generated using both the CTEQ ($R_{th} = 0.924 \pm 0.037$) and MRST ($R_{th} = 0.941 \pm 0.012$) PDF distributions. The uncertainties on the acceptance ratios are obtained from the error PDF sets using the previously described method. The uncertainty on the measured ratio is of the same order as the PDF uncertainties on the theoretical ratio, suggesting that a similar measurement with additional statistics would help to constrain the PDF models.

E. Differential Z Boson Cross Section

Measuring the differential boson production cross section over the full rapidity range can further improve PDF model constraints. The dilepton decay modes of the Z boson allow for precise measurements, since the backgrounds in these final states are small and the full event kinematics can be precisely reconstructed. The rapidity of the Z boson is closely related to the proton momentum fractions carried by the two colliding quarks. As shown in Figure 21, W or Z bosons are produced at high rapidity when the proton momentum fraction of one quark is significantly larger than that of the other. Therefore, the measured differential cross section at high rapidity is a good probe of the PDF distributions at high x_p.

DØ has made a preliminary measurement of the differential Z boson cross section based on a 337 pb^{-1} data sample. Using $Z \to ee$ candidate events, DØ reconstructs the differential cross section shown in Figure 22. The measured cross section is observed to agree well with the NNLO prediction. The measurement is currently statistics-limited but can be used to constrain PDF models using additional data.

F. W Boson Charge Asymmetry

A final measurement useful for constraining PDFs is the W boson charge asymmetry measurement. On average the u quarks inside the proton contain a higher fraction of the proton's momentum than the d quarks. Due to this imbalance, W^+ (W^-) bosons produced at the Tevatron have a net positive (negative) rapidity, as shown in Figure 23. The V-A structure of the electroweak couplings dictates the angular distribution of

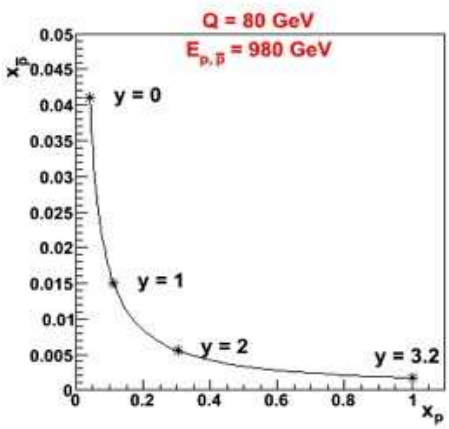

FIG. 21: The interacting partons' momentum fractions required to produce a W boson ($Q = 80$ GeV). The larger the difference between x_p and $x_{\bar{p}}$, the greater the rapidity of the produced boson.

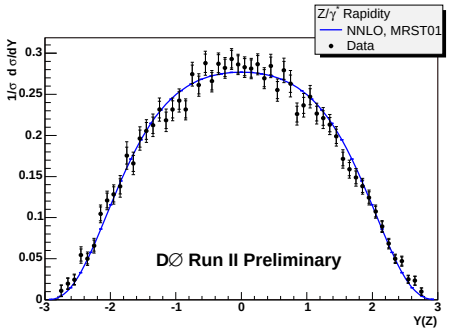

FIG. 22: Differential Z boson cross section measured by DØ as a function of boson rapidity. The measured cross section is in good agreement with a NNLO theoretical prediction based on MRST PDFs (solid line).

the leptons in the decays of the W bosons, which is preferentially opposite to the production asymmetry. As shown in Figure 23, the net effect of the decay asymmetry is to partially reduce the observable production asymmetry extracted from the lepton rapidity distributions. Because the production asymmetry originates from the imbalance of the momentum fractions carried by u and d quarks within the proton, charge asymmetry measurements provide constraints on the d/u ratio in the proton as a function of x_p.

Measurements are typically performed using the charged leptons from the W boson decays. The lepton asymmetry is defined as

$$A(\eta_\ell) = \frac{d\sigma_+/d\eta_\ell - d\sigma_-/d\eta_\ell}{d\sigma_+/d\eta_\ell + d\sigma_-/d\eta_\ell} = A(y_W) \otimes (V - A). \quad (22)$$

Both CDF and DØ have performed preliminary measurements of the lepton charge asymmetry. The key experimental issues are understanding forward lep-

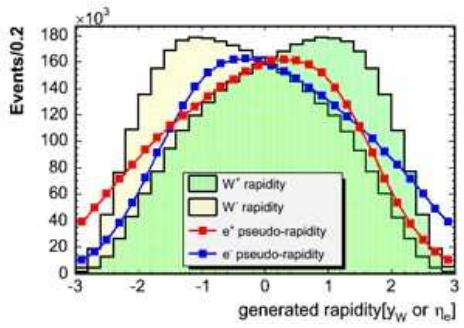

FIG. 23: Rapidity distributions of positively and negatively charged W bosons produced at the Tevatron, and the pseudorapidity distributions of the positively and negatively charged leptons produced in their decays.

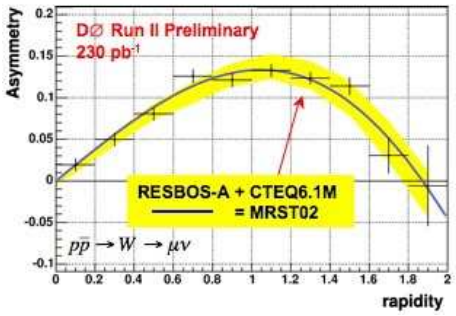

FIG. 24: DØ lepton charge asymmetry measurement based on $W \rightarrow \mu\nu$ events. The measurement is compared to a theoretical calculation based on the CTEQ and MRST PDF models.

ton identification and charge misidentification rates, which are needed to correct the observed asymmetry. A DØ measurement of the lepton charge asymmetry using $W \rightarrow \mu\nu$ events selected from a 230 pb^{-1} data sample is shown in Figure 24. The measured charge misidentification rates for this analysis are found to be below 10^{-4} out to muon pseudorapidities of 2. The measured asymmetry is compared to a theoretical prediction based on the CTEQ PDF model. The measurement is observed to have some sensitivity to PDFs even at the current level of statistical sensitivity. The CDF measurement based on $W \rightarrow e\nu$ events selected from a 170 pb^{-1} data sample are shown in Figure 25. Here the data is separated into two categories based on the E_T of the electron. Comparisons with theoretical predictions using the CTEQ PDF model illustrate the increased sensitivity of the high E_T events to PDF variations.

A new generation of Tevatron charge asymmetry analyses are currently under development, with the goal of fully exploiting the kinematic information in W events to directly reconstruct the underlying W boson production asymmetry. Applying a W mass constraint leads to two kinematic solutions that can

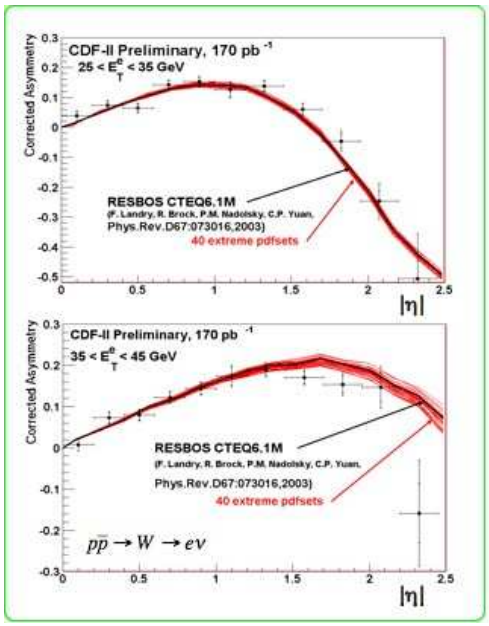

FIG. 25: CDF lepton charge asymmetry measurement based on $W \rightarrow e\nu$ events. The measurement is compared to a theoretical calculation based on the CTEQ PDF model.

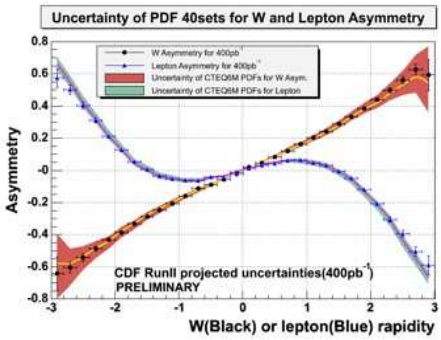

FIG. 26: Comparison of the potential PDF sensitivities for lepton charge asymmetry and W boson production asymmetry measurements made with a common set of simulated candidate events corresponding to a luminosity of 400 pb^{-1}.

be weighted by taking into account information about the production and decay of the W bosons. Potential dependencies on the input model are resolved through an iterative procedure. Preliminary CDF studies of this approach indicate significantly increased sensitivity to PDFs. The potential increase in sensitivity is illustrated in Figure 26, which shows a comparison of hypothetical lepton charge asymmetry and direct W boson charge asymmetry measurements based on a common set of candidate events obtained from a 400 pb^{-1} dataset.

V. CONCLUSIONS

The large samples of W and Z bosons being collected at the Tevatron accommodate a wide variety of electroweak measurements. In particular, the properties of the W boson can be measured with very high precision by the CDF and DØ experiments. In addition, detailed studies of boson production at the Tevatron can be used to constrain PDF models and provide important information about the boson production mechanisms. The analyses reported here are based on only a small fraction of the expected data, so there is significant room for improving the precision of the current measurements. It is important to note that obtaining similar precision results from the Large Hadron Collider (LHC) will be challenging and certainly require input (such as PDF constraints) from the Tevatron experiments.

[1] W.-M. Yao *et al.*, J. Phys. G**33**, 1 (2006), and references therein.

[2] Tevatron Electroweak Working Group (for the CDF and DØ Collaborations), "Combination of CDF and DØ results on the Mass of the Top Quark," hep-ex/060832.

[3] ZEUS Collaboration, "QCD and Electroweak analysis of the ZEUS NC and CC inclusive and jet cross sections," http://www-zeus.desy.de/public_results/publicsearch.html, ZEUS-prel-06-003.

[4] http://www-cdf.fnal.gov/physics/ewk/

[5] http://www-d0.fnal.gov/Run2Physics/wz/

[6] J. Campbell and K. Ellis, Phys. Rev. D**60**, 113006 (1999).

[7] http://www.phys.psu.edu/cteq

[8] http://www-spires.dur.ac.uk/hepdata/mrs.html

[9] P. Sutton, A. Martin, R. Roberts, and W. Stirling, Phys. Rev. D**45**, 2349 (1992).

[10] C. Hays *et al.*, Nucl. Instrum. Meth. Phys. Res. A **538**, 249 (2005).

[11] D. Acosta *et al.*, Phys. Rev. Lett. **94**, 091803 (2005).